ACS OMEGA

http://pubs.acs.org/journal/acsodf

Article

Development and Intensification of the Ethylene Process Utilizing a Catalytic Membrane Reactor

Abdulaziz S. Bin Naqyah[†] and Abdulrahman A. Al-Rabiah*[,†]

Cite This: *ACS Omega* 2022, 7, 28445−28458

Read Online

ACCESS | Metrics & More | Article Recommendations

ABSTRACT: Ethylene is considered the most important petrochemical constituent in the world today. It is currently produced via the thermal cracking process, which is generally expensive. Ethane dehydrogenation (EDH) is endothermic, and the thermodynamic equilibrium limits its conversion. The present study explores the viability of using a catalytic membrane reactor (MR) for ethylene production from EDH. The removal of hydrogen from the reaction zone using a palladium−silver (Pd−Ag) membrane has led to a high shift in the equilibrium conversion. The effects of operating conditions and reactor configurations on the ethane conversion were investigated. The ultimate ethane conversion was 22.2% when using the MR at 660 K and 300 kPa. The ethane conversion in the shell-side of the reactor increased to ∼99% when benzene hydrogenation was added as an auxiliary reaction in the tube-side of the reactor. Two new processes for ethylene production were developed for an annual capacity of 100,000 metric tons. Cryogenic distillation was required to separate ethylene from ethane if there is no auxiliary reaction. On the other hand, the ethylene process with cyclohexane as a byproduct does not require a refrigeration cycle system, and its economic analysis shows a return on investment of 34.4%, indicating that the process is a promising technology.

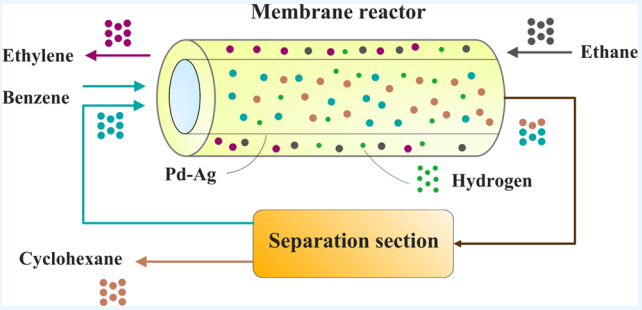

1. INTRODUCTION

Ethylene (C_2H_4) is the most important feedstock in the petrochemical industry.[1] It is used to produce plastics, fibers, and other added-value organic chemicals for consumption in different applications such as packaging and transportation.[2] Ethylene derivatives represent more than 70% of the petrochemical products, including high- and low-density polyethylene, ethylbenzene, styrene, polystyrene, acetaldehyde, ethylene glycol, acetic acid, vinyl acetate, and polyvinyl chloride.[3−5] Due to high consumption in many applications, the global ethylene capacity has increased in the last decade, and it is expected to reach 200 million tons by 2026.[6,7]

Thermal cracking of natural gas liquids or crude oil fractions in the presence of steam is the dominant route for ethylene production.[8,9] Thermal cracking accounts for 98% of the ethylene production worldwide.[10] Thermal cracking is energy-intensive and produces numerous byproducts, making it the most expensive in the petrochemical industry.[11−13] In general, the catalytic dehydrogenation of light alkanes is considered a promising technology due to its high selectivity toward ethylene.[14] Hydrogen is a byproduct of the dehydrogenation process, and it is considered a value-added component. The disadvantage of the catalytic dehydrogenation process is the thermodynamic limitations.[15] The dehydrogenation reaction is endothermic, and a high temperature is required to shift the reaction equilibrium forward.[16]

There are other ways to produce ethylene from gaseous feedstock. For instance, oxidative dehydrogenation (ODH) of ethane to ethylene in an oxygen ion transport membrane reactor (MR) has been studied.[17,18] The main drawback of ethane ODH is that the yield of ethylene is limited by the undesired total oxidation reactions of ethane and ethylene to carbon dioxide. Deep oxidation generates a large amount of heat that can cause temperature runaway of the fixed-bed reactor and even explosions.[19] The ODH of ethane has not been utilized yet on an industrial scale. In contrast, nonoxidative ethane dehydrogenation (EDH) can overcome most of the issues associated with ODH.[20] The main advantage of the catalytic EDH is that it enables ethylene production at lower temperatures than those required for the pyrolysis of ethane.[21]

The MR is a promising technology because it can overcome the reaction equilibrium limitation. The advantages of the MR include shifting the thermodynamic equilibrium, simultaneous

Received: May 19, 2022
Accepted: July 20, 2022
Published: August 4, 2022

https://doi.org/10.1021/acsomega.2c03130
ACS Omega 2022, 7, 28445−28458

reaction and separation processes in one unit, enhancement of the yield and selectivity, control of reactant distribution, and low operating costs.[22] The membrane catalytic reactor is still not thoroughly investigated despite its significant advantages. The technology is restricted to specific reactions, and it is not commercially used.[23]

In the catalytic dehydrogenation reactions, hydrogen is removed continuously from the MR.[24,25] The feasibility of dehydrogenation reactions with ceramic and metallic membranes has been demonstrated on a laboratory scale.[26] Palladium-based and silica-based inorganic membranes are among the most valuable hydrogen separation membranes due to their high hydrogen permeability and selectivity.[24]

Gobina, Hou, and Hughes[27] used a Pd−Ag membrane supported on a Vycor glass tube to perform experiments using ethane/N_2 as a feed gas mixture and palladium as a catalyst. The achieved ethane conversion using the MR was 18%, which is much higher than the equilibrium conversion of 3.5% at the same temperature and pressure. In other studies, the reported ethylene selectivity using the MR was ∼100%.[24,28]

Abashar and Al-Rabiah[22] investigated a rigorous two-dimensional mathematical model to simulate a bench-scale MR for EDH to produce ethylene with the aid of benzene hydrogenation to cyclohexane as an auxiliary reaction using a palladium-based membrane. Their study showed that the well-mixed pattern method significantly improved the reactor performance in terms of a high conversion, low operating temperature, and reduced total reactor length. Despite the enhanced results, the model was only implemented on one MR configuration where the two reactions occur in the tube-side of the reactor. Due to this configuration, benzene and cyclohexane were mixed with ethylene, which required further purification.

The present study aims to develop and integrate an ethylene process that utilizes MR technology. The catalytic MR is modeled and designed for ethylene production in two different configurations. The developed model is validated with previous experimental data under different operating conditions. The MR with an axillary reaction is configured such that the EDH reaction occurs in the shell-side of the reactor. In contrast, the exothermic reaction of the benzene hydrogenation reaction occurs in the tube-side of the reactor. Two schemes for ethylene production that utilize the MR are developed and compared from technical and economic aspects.

2. REACTION KINETICS

Ethylene can be produced from EDH through a catalytic process at lower temperatures compared to thermal cracking, which requires high temperatures. The dehydrogenation of ethane is an endothermic reaction, as shown in eq 1.

$$C_2H_6(g) \rightleftharpoons H_2(g) + C_2H_4(g)\ \Delta H_{298} = 137\ \text{kJ/mol} \quad (1)$$

Since the EDH reaction is endothermic, higher temperatures are required to attain a higher equilibrium conversion. On the other hand, the equilibrium conversion increases as the reaction pressure decreases according to Le Chatelier's principle.

The kinetic expression of EDH using a palladium catalyst is given by eq 2[27]

$$r_a = 4.39 \exp\left(-\frac{75{,}580}{RT}\right)\left[\frac{P_{C_2H_6} - P_{C_2H_4}P_{H_2}}{K_{eq}}\right] \quad (2)$$

where R is the universal gas constant (J mol^{-1} K^{-1}) and T is the reaction temperature (K). The equilibrium constant, K_{eq}, is a function of temperature T. K_{eq} is calculated from the standard heat of the reaction and the Gibbs free energy (ΔG°)[29]

$$\ln K_{eq} = -\frac{\Delta H^\circ}{RT} + \frac{\Delta a}{R}\ln T + \frac{\Delta b}{2R}T + \frac{\Delta c}{6R}T^2 + \frac{\Delta c}{6R}T^3 + \frac{\Delta d}{20R}T^4 + I \quad (3)$$

where ΔH° is the standard heat of the reaction (kJ/kg mol); a, b, c, and d are the activity coefficient values; and I at temperature T_0 is calculated as follows[29]

$$I = -\frac{\Delta H^\circ}{RT_0} + \frac{\Delta a}{R}\ln T_0 + \frac{\Delta b}{2R}T_0 + \frac{\Delta c}{6R}T_0^2 + \frac{\Delta c}{6R}T_0^3 + \frac{\Delta d}{20R}T_0^4 - \frac{\Delta G^\circ}{RT_0} \quad (4)$$

3. MATHEMATICAL MODEL DEVELOPMENT

A rigorous two-dimensional model was developed for the dehydrogenation of ethane. It is assumed that ethane entered the tube-side of the MR. A sweep gas is entered through the shell-side of the reactor as a countercurrent flow. The schematic diagram of a catalytic MR is shown in Figure 1. The model was developed based on the assumptions listed in Table 1.

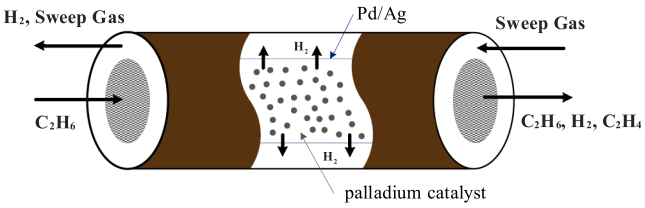

Figure 1. Schematic diagram of the MR.

Table 1. List of Assumptions Used for the MR Model

I.	plug-flow behavior under steady-state conditions.
II.	the pressure is constant along the feed side of the membrane.
III.	the heat transfer resistance between the catalyst particles and the bulk fluid is negligible.
IV.	counter-current flow configuration.
V.	isothermal system if no auxiliary reaction is added.
VI.	the effectiveness factor of the catalyst particles was taken as unity.

3.1. Tube-Side of the Reactor. To describe the mass transfer of components in the tube-side, the convective mass transfer in the axial direction, diffusion in the radial direction, and the chemical reaction are given in the following equations:[22,27]

•Tube-side: $0 < r < R_1$

$$\frac{\partial(u_l^t C_i^t)}{\partial l} = \varepsilon^t \frac{1}{r}\frac{\partial}{\partial r}\left(rD_{e_i}^t \frac{\partial C_i^t}{\partial r}\right) + \rho_{cat}^t(1-\varepsilon^t),\ \forall\ i \quad (5)$$

$$\rho_G^t C_p u_l^t \frac{\partial T^t}{\partial l} = \frac{1}{r}\frac{\partial}{\partial r}\left(\lambda_{ef}^t r_1 \frac{\partial T^t}{\partial r}\right) + \rho_{cat}^t(1-\varepsilon^t) \quad (6)$$

The boundary conditions are

https://doi.org/10.1021/acsomega.2c03130
ACS Omega 2022, 7, 28445−28458

$$l = 0,\ C_i^t = C_{in}^t,\ r = 0,\ \frac{\partial C_i^t}{\partial r} = 0;\ r = R_1$$

•Ceramic support: $R_1 < r < R_2$

$$\frac{\varepsilon^c}{r}\frac{\partial}{\partial r}\left(rD_{e_i}^c\frac{\partial C_i^c}{\partial r}\right) = 0,\ \forall\ i \tag{7}$$

$$\frac{1}{r}\frac{\partial}{\partial r}\left(\lambda^c r\frac{\partial T^c}{\partial r}\right) = 0, \tag{8}$$

$$r = R_2:\ \left.\frac{\partial C_i^c}{\partial r}\right|_{r=R_2} = 0,\ \forall\ i \neq H_2; \tag{9}$$

$$\text{for } H_2:\ D_{e_{H_2}}^c\varepsilon^c\left.\frac{\partial C_{H_2}^c}{\partial r}\right|_{r=R_2} = \left(\frac{Q_0}{\delta}\right)[\sqrt{P_{H_2}^c} - \sqrt{P_{H_2}^s}] \tag{10}$$

where u_l^t is the axial velocity in the tube-side (m/s); $C_i^{t,c}$ is the concentration of the ith component in the tube-side and the ceramic support (kmol/m^3); l is the reactor length (m); d is the diameter of the reactor (m); $\varepsilon^{t,c}$ is the porosity of the catalyst layer in the tube-side and the ceramic support; r is the radial coordinate in the catalyst layer (m); $D_{e_i}^t$ is the effective coefficient of radial diffusion of the ith component in the tube and the ceramic support (m^2/s); γ_{ij} is the stoichiometric coefficient of the ith component in the jth reaction; and δ is the membrane thickness (m).

3.2. Shell-Side of the Reactor. The convective mass transfer in the axial direction and the hydrogen flux across the membrane were considered with appropriate boundary conditions.

$$\frac{\partial(u_l^s C_i^s)}{\partial l} = \frac{Q'_{H_2}P_w}{S_{sc}} + \rho_{cat}^s(1-\varepsilon^s)\times\gamma_i r_a,\ \text{for } i = H_2$$

$$,\ Q'_{H_2} = \frac{Q_{H_2}}{A_m}, \tag{11}$$

$$Q'_{H_2} = Q_0\frac{Q_{H_2}}{A_m}[\sqrt{P_{H_2}^c} - \sqrt{P_{H_2}^s}] \tag{12}$$

The boundary conditions are

$$l = 0,\ C_i^s = C_{in}^s$$

where u_l^s is the axial velocity in the shell-side (m/s), C_i^s is the concentration of the ith component in the shell-side (kmol/m^3), l is the reactor length (m), ε^s is the porosity of the catalyst layer in the shell-side, Q'_{H_2} is the rate of penetration of H_2 through the membrane (kmol/s), S_{sc} is the surface area of the section, ρ_{cat}^t is the catalyst density in the tube-side (kg/m^3), γ_{ij} is the stoichiometric coefficient of the ith component in the jth reaction, P_w is the perimeter of the wall (m), Q_{H_2} is the rate of penetration of H_2 through the membrane (kmol/s), and A_m is the area of the membrane (m^2).

3.3. MR with an Auxiliary Reaction. The hydrogenation of benzene is used as an auxiliary reaction for shifting the equilibrium to increase the ethane conversion by removing hydrogen gas as the reaction proceeds forward to produce cyclohexane. In the tube-side of the MR, the benzene hydrogenation exothermic reaction provides the necessary heat for the endothermic reaction of catalytic EDH in the shell-side of the reactor. The exothermic reaction is placed in the tube-side of the MR to reduce the heat losses through the walls. On the other hand, if the exothermic reaction occurs in the shell-side, a part of the heat will be lost due to the radial convection heat transfer.

The exothermic hydrogenation reaction of benzene is as follows:[30]

$$C_6H_6(g) + 3H_2(g) \rightleftharpoons C_6H_{12}(g)\ \Delta H = -123.1\times10^3\ \text{J/mol} \tag{13}$$

The reaction rate of the benzene reaction using a nickel catalyst is described as follows[22]

$$r_b = 121.11\exp\left(-\frac{726.32}{RT}\right)K_B\left[\frac{P_{C_6H_6}P_{H_2}}{(1+K_BP_{C_6H_6})(P_{C_6H_6}+P_{H_2})}\right] \tag{14}$$

The adsorption equilibrium constant (K_B) is given by[22]

$$K_B = 788.0\exp\left(-\frac{363.16}{RT}\right) \tag{15}$$

The schematic diagram of the MR with an auxiliary reaction in the tube-side is shown in Figure 2.

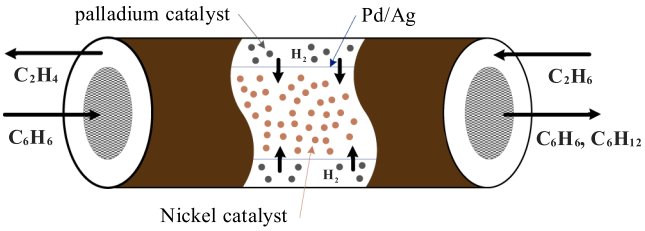

Figure 2. Schematic diagram of the MR with an auxiliary reaction in the tube-side.

3.4. Energy Balance. The energy balance of the MR is necessary to calculate the required heat for the EDH and determine the amount of benzene required for the exothermic reaction. The heat transfer between the tube and shell sides, the convective heat transfer in the axial direction, thermal conductivity in the radial direction, and the heat effect of the reactions were taken into account, as described by eq 16.

$$\frac{dT}{dl} = \frac{\frac{UA}{\rho}(T - T_a) + (r_a\Delta H_{rxn})}{\sum F_i C_{p_i}} \tag{16}$$

where

$$\frac{1}{U} = \frac{1}{h_1} + \frac{L}{\gamma} + \frac{1}{h_2} \tag{17}$$

where U is the overall heat transfer coefficient (W m^{-2} K^{-1}), C_{p_i} is the specific heat of the gas at a constant pressure of the ith component (J mol^{-1}), and A is the cross-sectional area (m^2). The thermal conductivity of the tube inside the MR (γ) equals 153.95 [(W/(m K)],[31] and h_1 and h_2 [W/(m^2 K)] are the inner and outer heat transfer coefficients, respectively. The convective heat transfer coefficients of gases vary in the tube, and their values are between 10 and 350 W/(m^2 K).[32]

The model equations were solved by PolyMath software based on Runge−Kutta−Fehlberg (RKF45), which can

https://doi.org/10.1021/acsomega.2c03130
ACS Omega 2022, 7, 28445−28458

evaluate the conversion based on the material and energy balance equations (i.e., eqs 5, 11, 16, and 17).

4. RESULTS AND DISCUSSION

The model of the catalytic MR was validated using the experimental data. Table 2 shows the input parameters used for the mathematical model of the MR.

Table 2. Input Parameters of the MR Model

parameter	value
reaction phase	gas
MR length (m)	0.15
catalyst bed diameter (m)	0.78
catalyst type	Pd/Ag
catalyst density (kg/m^3)	355
temperature range (K)	500−800
tube-side pressure range (kPa)	150−300
shell-side pressure (kPa)	101
catalyst bed porosity	0.5

The model validation was performed based on the operating conditions given in the study of Gobina et al.[27] Several runs were carried out to study the effect of the contact time on ethane conversion at 660 K and 128 kPa. The input data used for the MR model are the same as the experimental work. Figure 3 shows the model predictions and the experimental

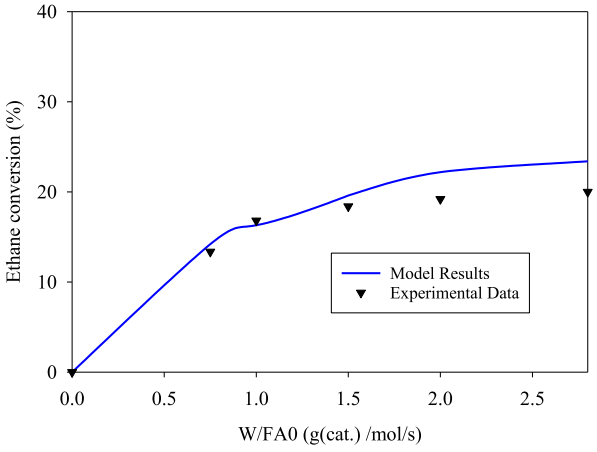

Figure 3. Model results and experimental data of ethane conversion using a MR.

data of the ethane conversion as a function of (W/F). (W/F) is defined as the ratio of the catalyst weight to the molar flow rate of the ethane feed.

Table 3 shows a comparison between the model and the experimental results of the data shown in Figure 3. The predictions obtained from the model showed that the conversion of ethane under different operating conditions was similar to the experimental conversion, with relative deviation values less than 17%.

A parametric study was carried out to investigate the influence of reaction conditions on the ethane conversion. The equilibrium reactor (REquil) model of Aspen Plus was used to calculate the equilibrium conversion of ethane at different temperatures and pressures, as shown in Figure 4.

The kinetics of the EDH reaction was investigated for a temperature range of 500−800 K. The tube-side operating

Table 3. Model Results and Experimental Data of Ethane Conversion Using a MR

sample	W/F$_{A0}$ (g$_{(cat.)}$/mol/s)	conv. (%) experimental results[27]	conv. (%) model results	relative deviation (%)
1	0.75	13.36	14.2	6.29
2	1	16.8	16.3	−2.98
3	1.5	18.4	19.6	6.52
4	2	19.2	22.2	15.63
5	2.8	20	23.4	17.00

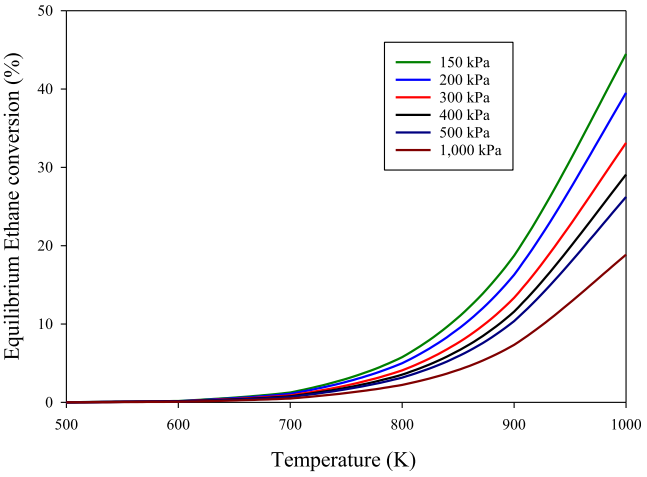

Figure 4. Equilibrium conversion of EDH.

pressure was varied between 150 and 300 kPa, while in the shell-side, the pressure was maintained at 101 kPa.

Figure 5 shows the effect of reaction temperature and pressure on the ethane conversion in the tube-side of the catalytic MR. The achieved ethane conversion was 29% at a temperature of 800 K and a pressure of 300 kPa. Note that the corresponding equilibrium conversion at the same temperature and pressure was ∼6%. This is because the MR separates and removes hydrogen from the feed stream, which improves the conversion. The pressure increase in the tube-side of the reactor increases the hydrogen permeation across the membrane. At the same time, the pressure increase moves the reaction backward according to Le Chatelier's principle. However, the net pressure effect in the system favors an increase in ethane conversion, as shown in Figure 5a. As the pressure increases, more hydrogen is permeated across the membrane, which allows the reaction to shift forward to increase the ethane conversion.

The effect of reaction pressure on the hydrogen stage cut is shown in Figure 5b. The stage cut is defined as the fraction of hydrogen that permeates through the membrane and is given by eq 18

$$\theta_{H_2} = \frac{\text{permeate flow}}{\text{feed flow}} \tag{18}$$

The increase in reaction pressure increases the driving force for the H_2 transfer across the membrane, which leads to greater hydrogen permeation. The maximum stage cut is at ∼680 K for all the pressure values tested, and after that, all the curves flatten out. The ethane conversion at a temperature of 680 K has achieved its maximum value, and thus, the stage cut is not affected by increasing the temperature above 680 K.

https://doi.org/10.1021/acsomega.2c03130
ACS Omega 2022, 7, 28445−28458

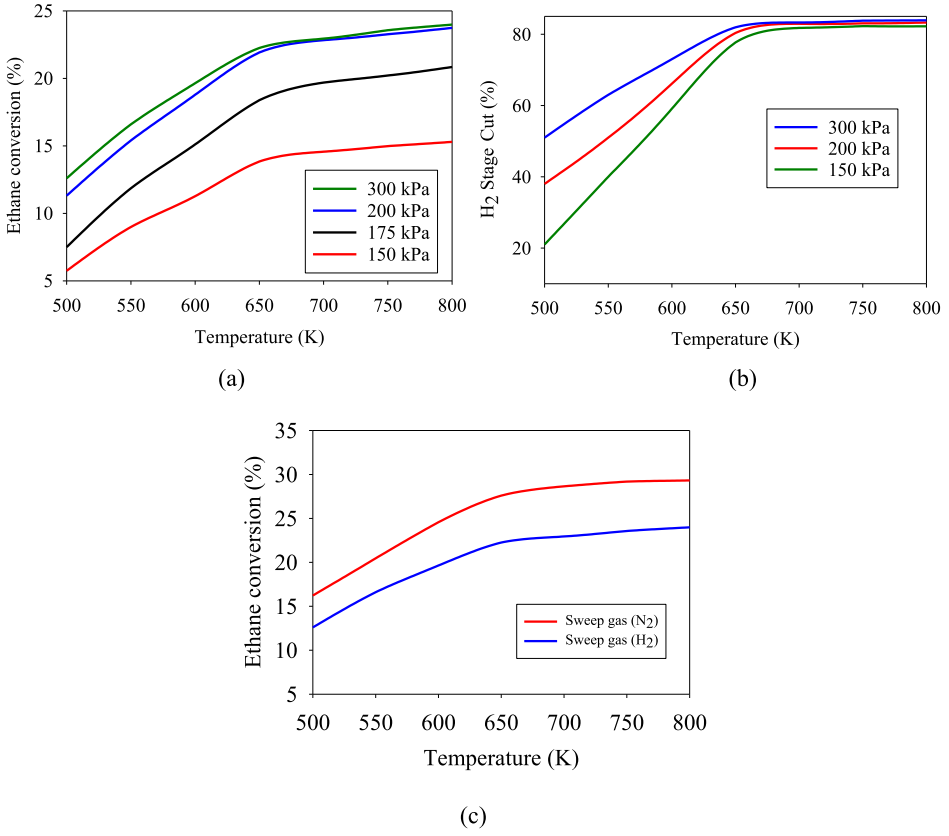

Figure 5. Effects of reaction temperature and pressure on the (a) ethane conversion and (b) hydrogen stage cut in the catalytic MR tube-side (c) when using different types of sweep gases at a tube-side pressure of 300 kPa.

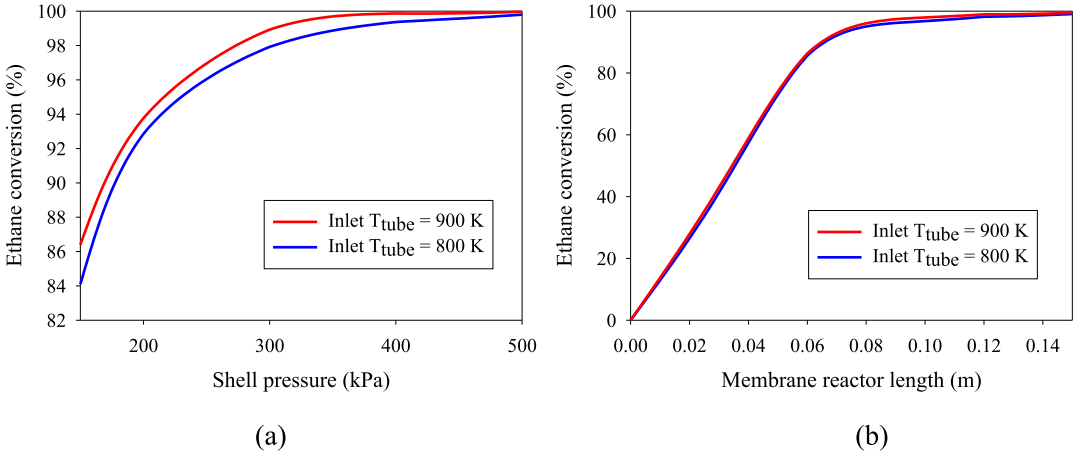

Figure 6. (a) Effects of reaction pressure and benzene inlet temperature on the ethane conversion in the shell-side and (b) ethane conversion along the MR length at different benzene inlet temperatures.

The effect of sweep gas type on the ethane conversion is shown in Figure 5c. The sweep gas minimizes the impact of the concentration−polarization phenomenon in the permeate side and thus increases the hydrogen flux through the membrane wall.[33] However, using hydrogen instead of nitrogen as a sweep gas in the permeate side of the membrane decreases the ethane conversion. This is clear since the hydrogen flux across the membrane is a function of the chemical potential driving force. The total pressure in the tube-side could be increased to overcome the decrease in the ethane conversion when using hydrogen as a sweep gas. In general, the driving force increases as the pressure difference between the tube and shell sides is increased.

Figure 6a shows the effects of shell-side pressure and inlet temperature of benzene on the ethane conversion when benzene hydrogenation is an auxiliary reaction. Benzene hydrogenation increases hydrogen permeation from the shell to the tube-side due to the hydrogen concentration gradient. The ethane conversion increased to ∼99% due to the high hydrogen flux to the tube-side of the reactor through the palladium−silver membrane. The maximum ethane conversion was 22.2% when the main reaction was used without an auxiliary reaction. The tube-side pressure was fixed at 101 kPa,

https://doi.org/10.1021/acsomega.2c03130
ACS Omega 2022, 7, 28445−28458

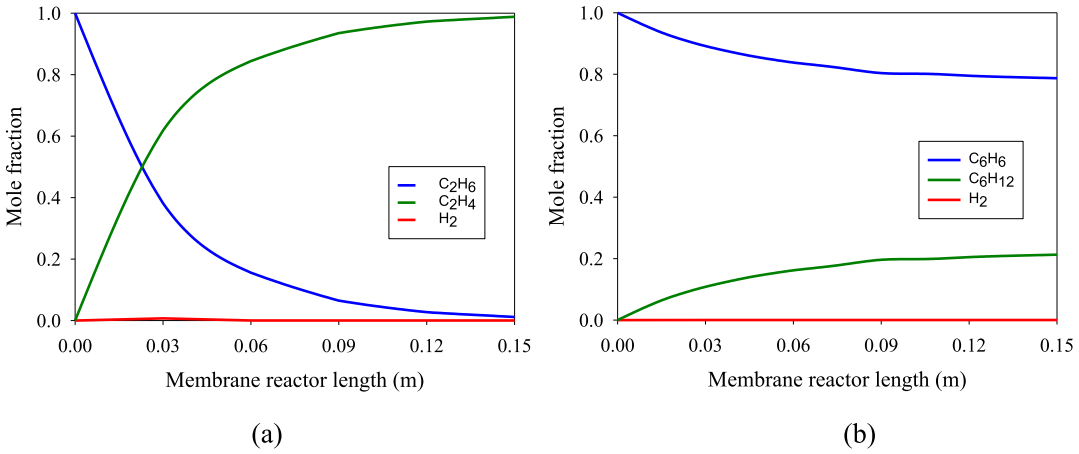

Figure 7. Compositions of component species at an ethane inlet temperature of 660 K, a benzene inlet temperature of 800 K, and a shell-side pressure of 300 kPa. (a) EDH in the shell-side and (b) benzene hydrogenation in the tube-side.

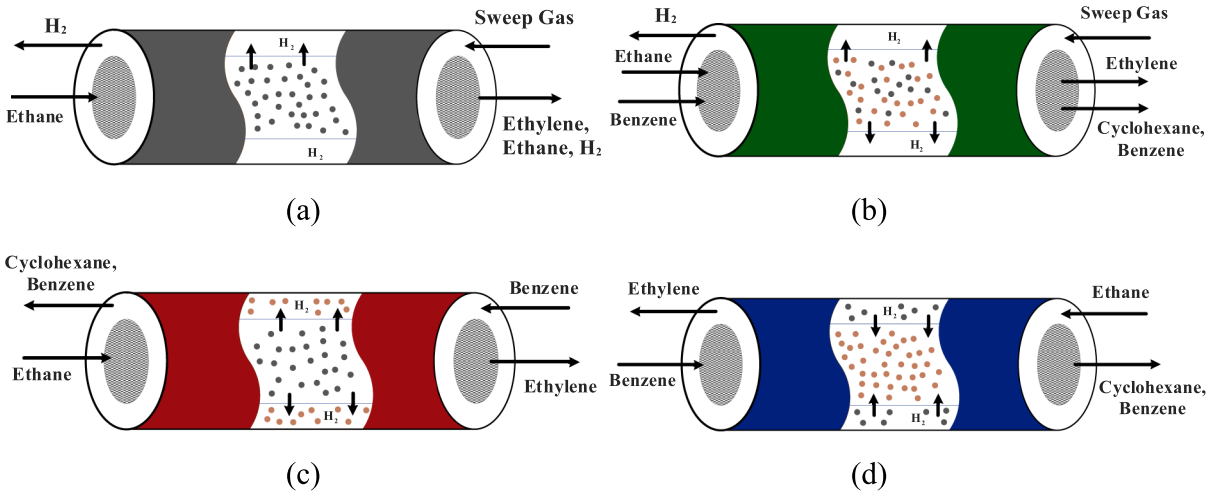

Figure 8. Possible configurations for the ethylene process: (a) EDH inside the tube-side, (b) EDH with benzene hydrogenation in the tube-side, (c) EDH in the tube-side with benzene hydrogenation in the shell-side, and (d) EDH in the shell-side with benzene hydrogenation in the tube-side.

and the inlet temperature of ethane was set at 660 K, and hydrogen was used as a sweep gas. The inlet temperature of benzene was studied at 800 K and 900 K.

The ethane conversion increases as the shell-side pressure increases for a fixed tube-side pressure of 101 kPa. When the shell-side pressure approaches 500 kPa, the ethane conversion approaches completion. The inlet temperature of benzene, which is above the ethane reaction temperature, slightly affects the ethane conversion.

Figure 6b shows the ethane conversion along the length of the MR at a shell-side pressure of 300 kPa and a temperature of 660 K. It is observed that the ethane conversion approaches completion at a membrane length of 0.14 m. The effect of the benzene inlet temperature is minimal.

Figure 7 shows the compositions of the component species along the length of the MR in the shell and tube sides, respectively. The ethane inlet temperature was fixed at 660 K with a shell-side pressure of 300 kPa. The benzene inlet temperature was fixed at 800 K with a tube-side pressure of 101 kPa. It is observed that the ethane conversion increases until completion toward the end of the shell-side length. On the other hand, the composition of hydrogen in both sides is low due to the high permeation flux through the membrane and the instantaneous reaction with benzene in the tube-side.

5. ETHYLENE PROCESS DEVELOPMENT

Simulation studies are required to identify the optimal configuration which provides the most significant economic advantage, and such studies are helpful in determining the operational limits for each process. The MR model used in this study was integrated with other process units utilizing the Soave−Redlich−Kwong (SRK) equation as the equation of state. The MR was linked to other parts of the process in the simulator. Equipment dimensions and operating conditions were evaluated by computer routines included with the Aspen Plus simulator. The simulation sequences pursued for evaluating the MR depend on the location of the catalytic EDH process. Figure 8 shows four possible configurations for ethylene production based on EDH using a MR. Figure 8a shows EDH that occurs inside the tube using hydrogen as a sweep gas. Figure 8b shows the dehydrogenation of ethane together with benzene hydrogenation that occurs in the tube-side of the reactor. The disadvantage of this configuration is the complicated separation of products and reactants. Figure 8c shows that EDH occurs inside the tube, while the hydrogenation of benzene is carried out in the shell-side. The drawback of this configuration is the heat loss due to the radial convection. The configuration shown in Figure 8d is the

https://doi.org/10.1021/acsomega.2c03130
ACS Omega 2022, 7, 28445−28458

opposite of Figure 8c. The current study considers the configurations of Figure 8a,d for the aforementioned reasons. Table 4 lists the process parameters and assumptions for each process. Hydrogen is used as a sweep gas. The reason for selecting hydrogen as a sweep gas for ethylene process is to avoid a costly cryogenic separation of hydrogen (byproduct) from nitrogen as a sweep gas.

Table 4. Process Parameters and Assumptions for the Ethylene Process

	value	
parameter	single reaction	with an axillary reaction
plant capacity, metrictons/year	100,000	100,000
product purity, mol %	99.9	99.9
byproduct, mol %	N/A	99.8
working hours, hr/year	8000	8000
technology	MR	MR
catalyst type	Palladium	Palladium
membrane type	Pd−Ag	Pd−Ag
ethane feed temperature, K	298	298
ethane feed pressure, kPa	270	270
benzene feed temperature, K	N/A	298
benzene feed pressure, kPa	N/A	130
ethane−benzene ratio	N/A	1:4
shell-side T_{inlet}, K	N/A	660
tube-side T_{inlet}, K	660	873
shell-side pressure, kPa	110	300
tube-side pressure, kPa	300	110
Sweep gas	H_2	N/A

5.1. Ethylene Process without an Auxiliary Reaction. A new process for ethylene production based on a catalytic MR was developed and simulated using Aspen Plus, and it is shown in Figure 9. The annual production capacity of the plant is 100,000 metric tons of 99.9 mol % ethylene.

Figure 9 shows the process flow diagram of the ethylene process based on a MR. An ethane feed (stream 1) is entered at 298 K and 270 kPa and mixed with the recycled ethane (stream 12). The mixed stream (stream 2) is compressed in C-101 and sent to a furnace, H-101, to increase the feed temperature. The total ethane feed enters the MR at 660 K and 400 kPa. In the MR, R-101, 22.2% of ethane is converted to ethylene and hydrogen. Hydrogen, and traces of ethane and ethylene (stream 5) permeate through the membrane to the shell-side of the MR. The retentate stream (stream 8) leaves the tube-side of the MR and is sent to a cooler, E-101. The product stream consisting of ethane and ethylene is sent to a distillation column, T-101, to separate ethylene from ethane. Ethylene is separated as a distillate (stream 10), while ethane is separated as the bottom stream (stream 11). The recycle stream is heated in E-103 before mixing with the ethane feed.

Heat integration of the ethylene process is essential for an efficient and optimal design. The base case ethylene process was heat integrated, as shown in Figure 10. The heat integration of the ethylene process was performed using the Aspen Energy Analyzer. The energy requirements of the ethylene process to satisfy the heating and cooling demands were determined.

The final heat exchanger network of the ethylene process is shown in Figure 11a. The network's blue and red lines denote the cold and hot streams, respectively. From Figure 10, it can be seen that the ethane feed (stream 3) is heated using hydrogen (stream 11) that leaves the shell-side of the MR, and the feed is further heated using the ethylene product (stream 7) that leaves the tube-side of the MR. The product (stream 8) is cooled using recycled ethane (stream 14). A considerable proportion of the process operating costs is attributed to the heating and cooling duties, which can be minimized using heat integration. In the base case design, the available energy savings were identified by comparing the actual energy demands with the energy targets. Figure 11b shows the actual energy consumption against the energy targets of the hot and cold utilities. The actual energy of the integrated process is almost identical to the energy targets. This indicates that the heat exchanger network is very efficient, and there is no gap for further energy reduction.

Table 5 shows the process stream information of the integrated ethylene process. The refrigeration system of the ethylene plant is shown in Figure 12, and ethylene is used as a refrigerant. The refrigerant (S1) is compressed in C-101 to 1800 kPa before passing through three coolers (E-101, E-102, and E-103). The refrigerant temperature is reduced from 289 to 183 K, where its phase is changed from vapor to liquid. The refrigerant is used to condense ethylene in the distillation condenser (E-105). After leaving the distillation condenser, the refrigerant temperature is increased to 189 K. The refrigerant is cooled and compressed to pass through the condenser.

5.2. Ethylene Process with an Auxiliary Reaction. A process for ethylene production using a catalytic MR with an auxiliary reaction was developed. The process parameters and assumptions of the ethylene process with an auxiliary reaction are listed in Table 4. Aspen Plus was used to simulate the process for an annual plant capacity of 100,000 metric tons with an ethylene purity of 99.9 mol %. A catalytic benzene hydrogenation process with a benzene−ethane feed ratio of 4:1 is used as an auxiliary reaction to supply heat to EDH and shift the thermodynamic equilibrium in the forward direction by consuming hydrogen in the tube-side of the reactor. Figure 13 shows the developed flowsheet of the ethylene process with

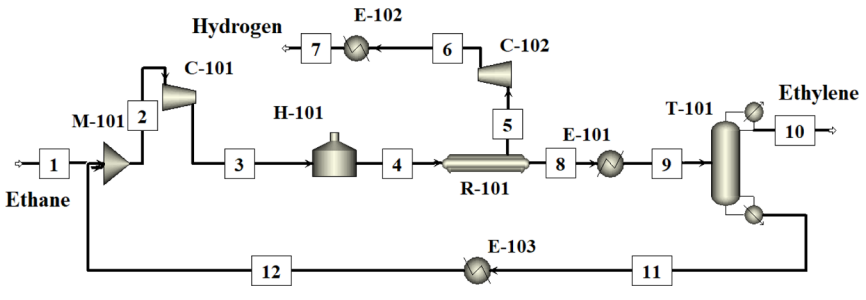

Figure 9. Ethylene process flow diagram using a MR.

https://doi.org/10.1021/acsomega.2c03130
ACS Omega 2022, 7, 28445−28458

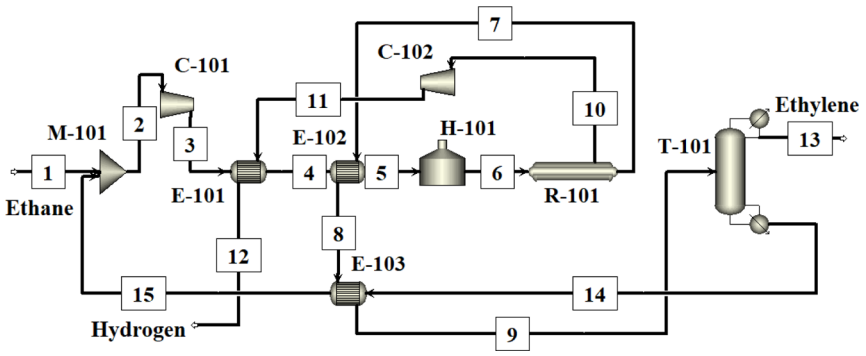

Figure 10. Integrated ethylene process using a MR.

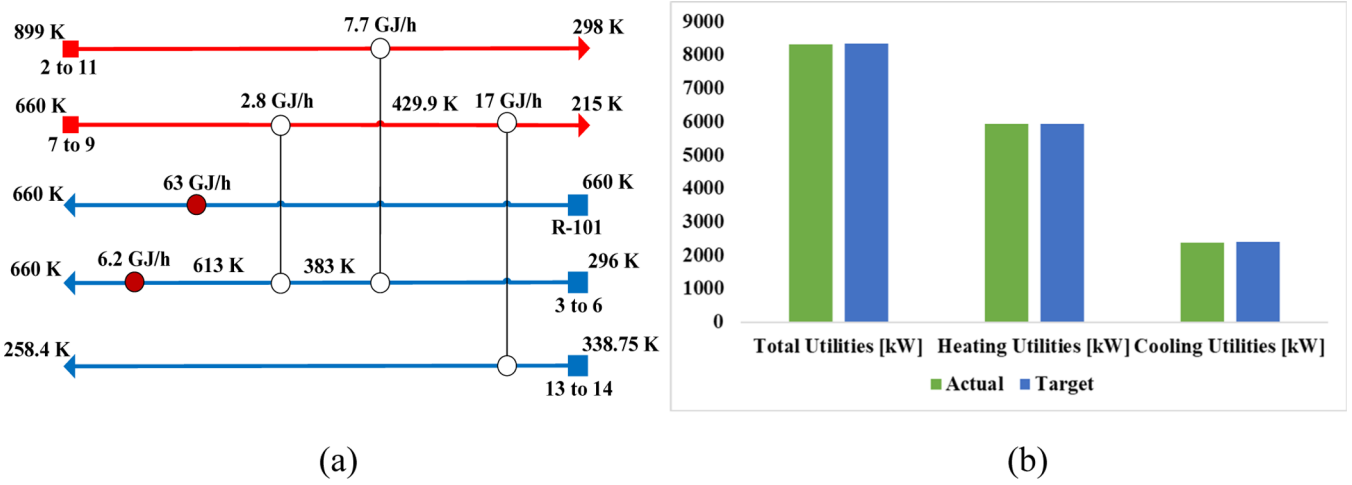

Figure 11. (a) Heat exchanger network for the main streams of the ethylene process and (b) actual and target energies of hot and cold utilities of the ethylene process.

Table 5. Stream Information of the Integrated Ethylene Process Using the Catalytic MR

stream no.	1	2	3	4	5	6	7
temperature, K	298.00	269.07	296.16	385.82	615.49	660.00	660.00
pressure, kPa	270.00	270.00	440.00	430.00	430.00	400.00	300.00
mole flow, kmol/h	446.00	2003.07	2003.07	2003.07	2003.07	2006.41	2006.26
mass flow, kg/h	13411.10	60230.69	60230.69	60230.69	60230.69	60331.18	59427.61
component mole flow, kmol/h							
ethane	446.00	2002.62	2002.62	2002.62	2002.62	2005.96	1560.48
ethylene	0.00	0.45	0.45	0.45	0.45	0.45	445.73
hydrogen	0.00	0.00	0.00	0.00	0.00	0.00	0.04
stream no.	8	9	10	11	12	13	15
temperature, K	430.00	215.00	660.11	899.23	298.00	188.29	258.82
pressure, kPa	290.00	290.00	110.00	300.00	290.00	270.00	290.00
mole flow, kmol/h	2006.26	2006.26	445.48	445.48	445.48	1565.07	1565.07
mass flow, kg/h	59427.61	59427.61	903.57	903.57	903.57	47060.19	47060.19
component mole flow, kmol/h							
ethane	1560.48	1560.48	0.16	0.16	0.16	1564.62	1564.62
ethylene	445.73	445.73	0.04	0.04	0.04	0.45	0.45
hydrogen	0.04	0.04	445.28	445.28	445.28	0.00	0.00

cyclohexane as a byproduct. The ethane feed with a flow rate of 445.72 kmol/h enters the process at a temperature of 298 K and a pressure of 270 kPa. The feed stream is compressed to 400 kPa in C-101. The feed is heated to 660 K in E-101 before sending it to the MR (R-101). The dehydrogenation of ethane is an endothermic reaction that takes place in the shell-side of the reactor. Benzene enters the tube-side of the MR in a counter-current flow, and the heat from the exothermic reaction of benzene hydrogenation is transferred to the shell-side of the reactor.

The ethane conversion increased from 22.2% in the MR with a main ethane reaction to ~99% after adding the auxiliary reaction. The ethylene product is cooled and sent for utilization in other industries. Benzene and cyclohexane are

https://doi.org/10.1021/acsomega.2c03130
ACS Omega 2022, 7, 28445−28458

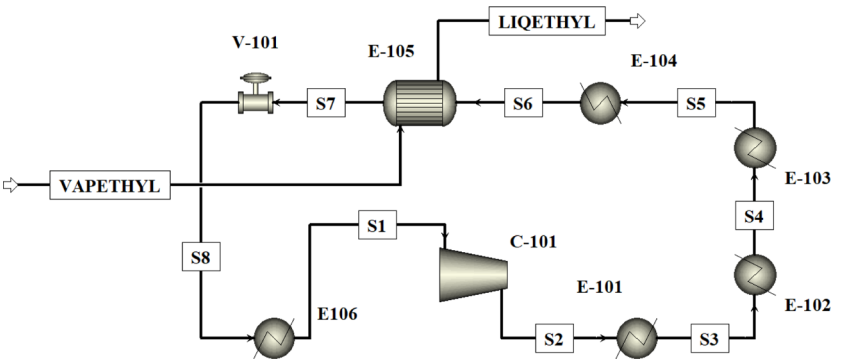

Figure 12. Refrigeration system of the ethylene plant.

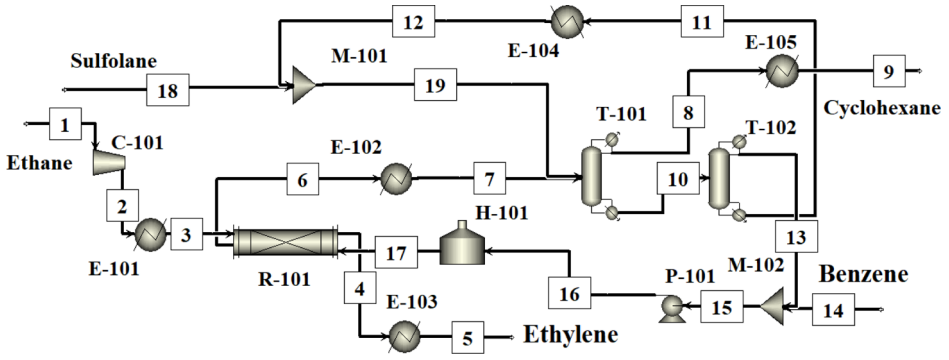

Figure 13. Process flow diagram of the MR ethylene process with an auxiliary reaction.

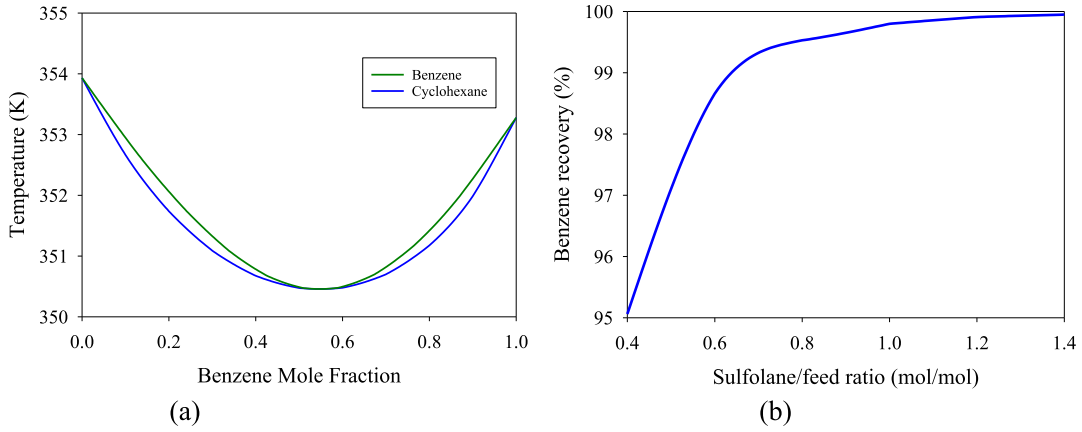

Figure 14. (a) VLE data of benzene−cyclohexane at 101 kPa and (b) benzene recovery as a function of the sulfolane−feed ratio.

cooled in E-102 and sent to the purification section to separate cyclohexane as a byproduct. Benzene and cyclohexane form an azeotropic mixture. Figure 14a shows the vapor−liquid equilibrium (VLE) data of benzene−cyclohexane at 100 kPa. The azeotropic mixture (stream 6) is sent to an extractive distillation (T-101), where sulfolane is used as a solvent. An extractive distillation column (T-101) was designed with 34 stages. Another column (T-102) was designed for solvent recovery, and it consists of 77 stages. The amount of the solvent was determined for a feed mixture having 45 mol % benzene and 55 mol % cyclohexane. Figure 14b shows how the recovery of benzene changes with the solvent to feed ratio. When the solvent to feed ratio is 1.21, a recovery of ∼99.9% benzene can be achieved. The byproduct, cyclohexane, is separated at the top of the extractive distillation column. The cyclohexane is cooled in E-105 before being sent to product storage.

The bottom stream from the extractive distillation is sent to the recovery column (T-102) where benzene is separated at the top of the column and recycled and mixed with the fresh benzene feed. Sulfolane is separated as a bottom stream and recycled back to the extractive distillation (T-101).

The ethylene process with an auxiliary reaction was integrated to reduce energy consumption. The heat exchangers E-101 and E-102 are used for cooling stream 4 by heating stream 2 and stream 7. The optimized ethylene process with an auxiliary reaction using heat integration is shown in Figure 15.

The heat exchanger network selected for the ethylene process is shown in Figure 16a. Mass and energy balances were determined for the integrated ethylene process using an auxiliary reaction. The actual energy consumption against the

https://doi.org/10.1021/acsomega.2c03130
ACS Omega 2022, 7, 28445−28458

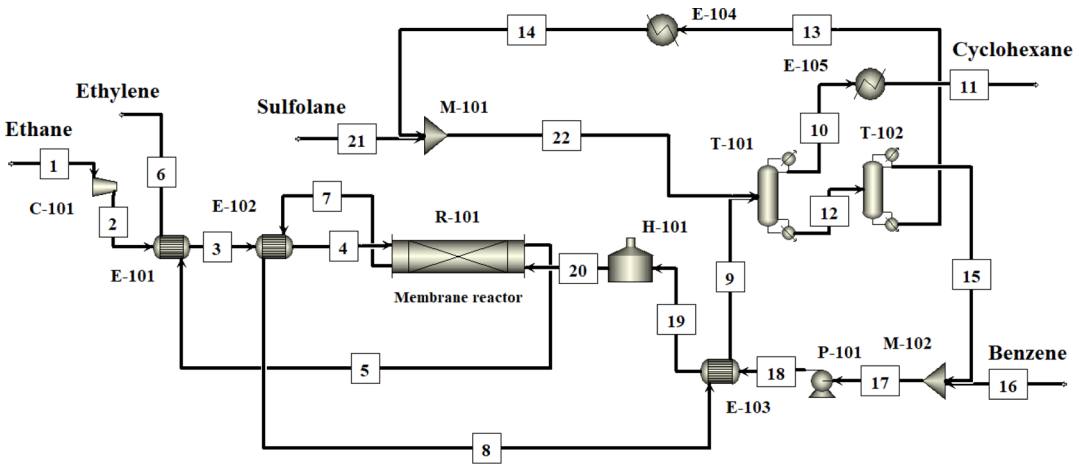

Figure 15. Integrated ethylene process using a MR with an auxiliary reaction.

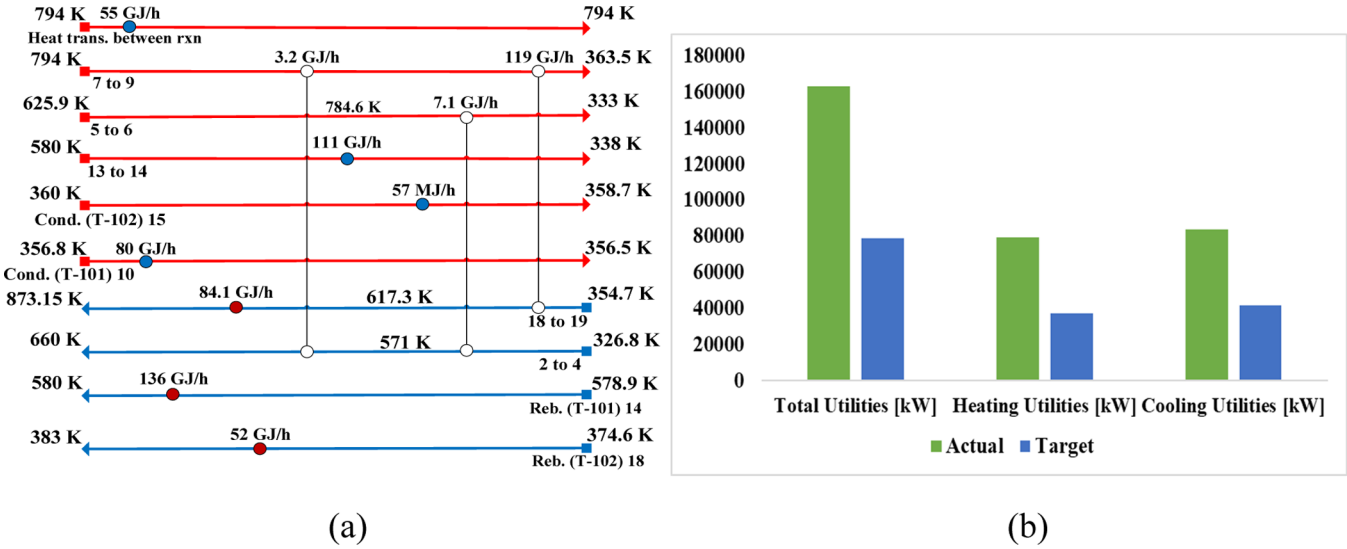

Figure 16. (a) Heat exchanger network for the ethylene production with cyclohexane and (b) actual and target energies of the ethylene process with cyclohexane.

energy targets for the modified process is shown in Figure 16b. The data relating to this process are given in Table 6.

6. PROCESS ECONOMICS

An economic analysis was performed to evaluate the feasibility of the ethylene process using the catalytic MR, and a comparison study was carried out for the process with and without an auxiliary reaction.

Aspen Process Economic Analyzer (APEA) was used to estimate the capital and operating costs based on the equipment module costing method. The direct and indirect process expenses were included in the capital cost calculations. The return on investment (ROI) and the payout period were used to evaluate the process's profitability. The key assumptions used in the techno-economic evaluation are given in Table 7.

The economic indicators were calculated for the integrated ethylene process, both with the main reaction and an auxiliary reaction. The economic results for both processes are given in Table 8. The process with an auxiliary reaction appears more economically feasible compared to the main reaction, which includes a refrigeration system that is needed for ethane–ethylene separation. In contrast, adding an auxiliary hydrogenation reaction to the MR increased the ethane conversion to ~99%, and it assisted in eliminating the refrigeration system and resulted in a promising technology.

The Process Economic Report 29H (Ethylene via Ethane Steam Cracking) published by IHS Chemical in December 2014 shows a total fixed capital cost of $2.245B for a 1.5 million metric tons per annum (MMTA) ethane cracker.[34] The Chemical Engineering Plant Cost Index (CEPCI) was used to update the plant costs in 2021 as a reference year (CEPCI = 699.97),[35] resulting in a capex intensity of $1,819/MT. The capex intensity of the ethylene process based on the MR is $1,683/MT. On the other hand, when EDH is associated with an auxiliary reaction (benzene hydrogenation), the capex intensity is $815/MT. This indicates that the capex of the auxiliary configuration is about 45% of that of the conventional steam cracker due to the elimination of the refrigeration system.

For the MR, the calculated area (m^2) is determined by estimating the driving force over the membrane. The average driving force over the membrane is multiplied by a hydrogen permeability of 3.14×10^{-13} (kg mol m/m^2 s $Pa^{0.5}$) at 660 K,[22]

https://doi.org/10.1021/acsomega.2c03130
ACS Omega 2022, 7, 28445−28458

Table 6. Stream Information of the Integrated Ethylene Process with an Auxiliary Reaction

stream no.	1	4	5	6	7	9	11
temperature, K	298.15	660.00	528.15	333.15	794.30	363.65	308.15
pressure, kPa	270.00	500.00	400.00	270.00	150.00	140.00	110.00
mole flow, kmol/h	445.72	445.72	445.76	445.76	1800.47	1800.02	148.36
mass flow, kg/h	13402.6	13402.6	12505.7	12505.7	141504.8	141503.9	12484.9
component mole flow, kmol/h							
ethane	445.72	445.72	0.71	0.71	0.00	0.00	0.00
ethylene	0.00	0.00	445.01	445.01	0.00	0.00	0.00
hydrogen	0.00	0.00	0.04	0.04	0.44	0.00	0.00
benzene	0.00	0.00	0.00	0.00	1651.62	1651.62	0.15
cyclohexane	0.00	0.00	0.00	0.00	148.40	148.40	148.21
sulfolane	0.00	0.00	0.00	0.00	0.00	0.00	0.00
stream no.	12	14	16	17	20	21	22
temperature, K	382.89	338.15	298.15	354.14	873.15	338.15	338.15
pressure, kPa	140.00	130.00	130.00	130.00	150.00	120.00	120.00
mole flow, kmol/h	3672.68	2021.02	148.36	1800.02	1800.02	0.00	2021.02
mass flow, kg/h	371888.5	242869.5	11588.6	140607.6	140607.6	0.02	242869.6
component mole flow, kmol/h							
ethane	0.00	0.00	0.00	0.00	0.00	0.00	0.00
ethylene	0.00	0.00	0.00	0.00	0.00	0.00	0.00
hydrogen	0.00	0.00	0.00	0.00	0.00	0.00	0.00
benzene	1651.49	0.02	148.36	1799.83	1799.83	0.00	0.02
cyclohexane	0.19	0.00	0.00	0.19	0.19	0.00	0.00
sulfolane	2021.00	2021.00	0.00	0.00	0.00	0.00	2021.00

Table 7. Key Assumptions Used in the Economic-Technical Assessment[36−38]

parameter	result	parameter	result
year of evaluation	2021	medium-pressure steam, $/GJ	2.5
length of the start-up period, week	20	high-pressure steam, $/GJ	4.25
plant lifetime, year	10	cooling water, $/m^3	1.0
operation hours per year	8000	ethane price, $/kg	0.15
tax rate, %	35	ethylene price, $/kg	1.08
interest rate, %	15	hydrogen price, $/kg	0.5
salvage value, %	20	benzene price, $/kg	0.95
electricity, $/MWhr	48	cyclohexane price, $/kg	1.12
low-pressure steam, $/GJ	1.9	sulfolane price, $/kg	20.00
palladium, $/g	19.6	MR (2021), $ million	2.07

Table 8. Summary of Economic Results for the Ethylene Process without and with an Auxiliary Reaction

	results	
parameter	single reaction	with an axillary reaction
equipment costs, $	25,832,000	12,473,000
fixed capital investment, $	143,035,000	69,328,000
working capital, $	25,258,000	12,238,000
total Capital Investment, $	168,293,000	81,538,000
raw material costs, $/year	15,760,000	105,440,000
product revenue, $/Year	111,610,000	219,778,000
total utility costs, $/year	15,756,000	7,720,000
payout period, year	5.5	2.7
ROI, %	6.9	34.4

where the palladium−silver alloy film thickness is 6.0 μm, which leads to a total membrane area of 1945 m^2.

The cost distribution of the process equipment for the ethylene process with and without an auxiliary reaction is shown in Figure 17. A sensitivity analysis was performed to evaluate the effect of raw material prices and product selling prices on the ROI, as shown in Figure 18. A three-dimensional graph was drawn to represent the ROI change against ethane, ethylene, and cyclohexane prices. The ultimate ROI is attained when the ethylene and cyclohexane prices are more than 1.1 $/kg.

7. CONCLUSIONS

The work presented in this study investigated various aspects of ethylene production based on a MR for the catalytic ethane reaction. The MR is based on a palladium catalyst and a Pd−Ag membrane. Two ethylene processes have been developed and integrated. The first ethylene process is based on EDH, which occurs in the tube-side of the reactor with an ultimate ethane conversion of 22.2%. This ethylene process requires a refrigeration system for ethane−ethylene separation using a cryogenic distillation column. In addition, this process is energy-intensive and capital expensive. The second developed ethylene process is based on EDH with an additional auxiliary reaction of benzene hydrogenation. Benzene hydrogenation is highly exothermic and can provide the necessary heat for the endothermic reaction of EDH. In addition, the hydrogenation reaction, which is placed in the tube-side, is used to increase the permeation of hydrogen through the membrane. Cyclohexane is a valuable byproduct and has various applications in different industries. The dehydrogenation of ethane is placed in the shell-side of the reactor to absorb all heat generated in the tube-side of the MR through the exothermic auxiliary reaction. The achieved conversion of ethane with an auxiliary reaction is ∼99%. Ethylene that exists in the shell-side of the MR is of the highest purity and does not need further purification. An economic evaluation was performed for both developed ethylene processes with an annual plant capacity of 100,000 metric tons and a polymer grade ethylene purity of 99.9 wt %. The economic analysis showed that the ethylene process with an auxiliary reaction is favored as compared to the

https://doi.org/10.1021/acsomega.2c03130
ACS Omega 2022, 7, 28445−28458

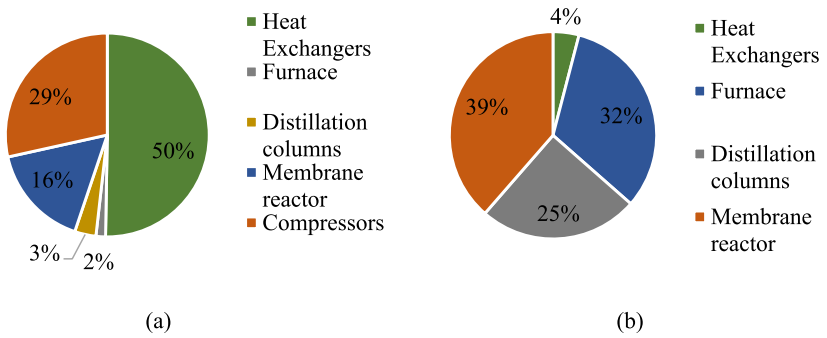

Figure 17. Equipment cost distribution for the ethylene process with (a) a single reaction and (b) an auxiliary reaction.

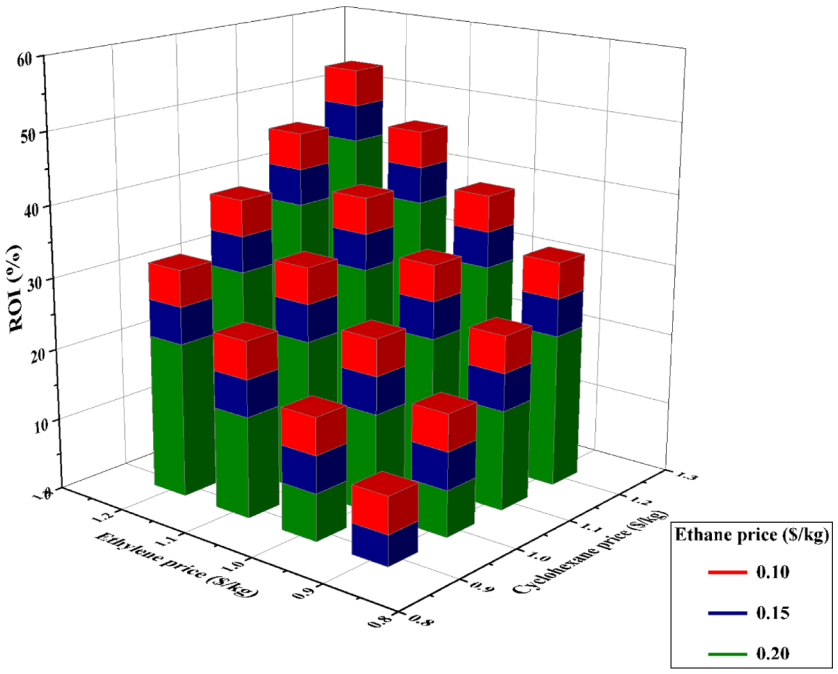

Figure 18. Effects of ethane, ethylene, and cyclohexane prices on the ROI for the ethylene process based on a MR with an auxiliary reaction.

ethylene process without the auxiliary reaction. The ROI and the payout period of the ethylene process with the auxiliary reaction are 34.4% and 2.7 years, respectively.

AUTHOR INFORMATION

Corresponding Author

Abdulrahman A. Al-Rabiah − *Chemical Engineering Department, College of Engineering, King Saud University, Riyadh 11421, Saudi Arabia;* orcid.org/0000-0001-5213-3209; Phone: +966 (11) 4676844; Email: arabiah@ksu.edu.sa; Fax: +966 (11) 4678770

Author

Abdulaziz S. Bin Naqyah − *Chemical Engineering Department, College of Engineering, King Saud University, Riyadh 11421, Saudi Arabia*

Complete contact information is available at: https://pubs.acs.org/10.1021/acsomega.2c03130

Author Contributions

†A.A.A.-R. and A.S.B.N. contributed equally to this work.

Notes

The authors declare no competing financial interest.

ACKNOWLEDGMENTS

This project was supported by King Saud University, Deanship of Scientific Research, College of Engineering Research Center.

NOMENCLATURES

A	cross-sectional area (m^2)
$C_i^{t,s,c}$	concentrations, kmol m^{-3}
C_p	specific heat of the gas at constant pressure (J mol^{-1})
D	tube diameter (m)
D_p	catalyst diameter (m)
$D_{e_i}^{t,c}$	effective coefficient of radial diffusion of component i, m^2 s^{-1}
D_{ij}	molecular diffusivity for component i in a binary mixture of i and j, m^2 s^{-1}
$D_m^{t,c}$	coefficient of molecular diffusion, m^2 s^{-1}
D_{kn}	Knudsen diffusion coefficient, m^2 s^{-1}
E_a	activation energy [J mol^{-1}]
H_i	heat transfer coefficient between the reaction side and reactor wall (W m^{-2} K^{-1})
H_o	heat transfer coefficient between the cooling side and reactor wall (W m^{-2} K^{-1})
ΔH	heat of the reaction (J mol^{-1})
k	rate constant (mol m^{-3} Pa^{-1} s^{-1})

https://doi.org/10.1021/acsomega.2c03130
ACS Omega 2022, 7, 28445−28458

K_{eq}	reaction equilibrium constant (mol m^{-3})
K_w	thermal conductivity of the reactor wall (W m^{-1} K^{-1})
k	kinetic constant, g^{-1} min^{-1}
k_0	pre-exponential factor of the kinetic constant, g^{-1} min^{-1}
K_B	adsorption constant
L	reactor length, m
P, P^o, P_i	pressure, standard pressure, and partial pressure, Pa
Q	membrane flux, mol m^{-2} Pa^{-1} s^{-1}
$r_{1,2}$	radial coordinate into the fixed bed catalyst and in the ceramic support, m
$r_{a,b}$	reaction rate, min^{-1}
R	ideal gas constant, J mol^{-1} K^{-1}
T	temperature, K
T_{shell}	shell-side temperature, K
T_{tube}	tube-side temperature, K
U	overall heat transfer coefficient, W m^{-2} K^{-1}
$U_l^{t,s}$	axial velocity, m s^{-1}
V	volume (m^3)
x	molar fraction
X_c	molar reaction conversion
z	axial reactor coordinate (m)
μ	viscosity of the fluid phase (kg m^{-1} s^{-1})
ρ	density of the fluid phase (kg m^{-3})
ρ_k	density of the catalytic bed (kg m^{-3})
η	effectiveness factor
π	overall membrane permeance (mol m^{-2} s^{-1})
$\varepsilon^{t,s,c}$	porosity of the catalyst layer (tube- and shell-side) and ceramic support
γ	thermal conductivity of the catalytic MR (W m^{-1} K^{-1})
γ_{ij}	stoichiometric coefficient for *i*-component into *j*-reaction
θ_{H_2}	hydrogen stage cut

REFERENCES

(1) Cheng, Y. W.; Chong, C. C.; Cheng, C. K.; Ng, K. H.; Witoon, T.; Juan, J. C. Ethylene Production from Ethanol Dehydration over Mesoporous SBA-15 Catalyst Derived from Palm Oil Clinker Waste. *J. Cleaner Prod.* **2020**, *249*, 119323.

(2) Sami, M. *PETROCHEMICAL*, 2001.

(3) Rossetti, I.; Compagnoni, M.; Finocchio, E.; Ramis, G.; Di Michele, A.; Millot, Y.; Dzwigaj, S. Ethylene Production via Catalytic Dehydration of Diluted Bioethanol: A Step towards an Integrated Biorefinery. *Appl. Catal., B* **2017**, *210*, 407−420.

(4) Gao, Y.; Neal, L.; Ding, D.; Wu, W.; Baroi, C.; Gaffney, A. M.; Li, F. Recent Advances in Intensified Ethylene Production—A Review. *ACS Catal.* **2019**, *9*, 8592−8621.

(5) Litmus, A. The, T. F. O. R. Ethylene: A Litmus Test for the Chemical Industry. Gulf Petrochemicals and Chemicals Association, 2019, No. November, 8.

(6) Holmvik, G.; Brooks, B.; Allen, K.; Sher, R.; Zhang, M.; Hays, K.; Cambeiro, M.; Niazi, S.; Tseng, T.; Price, S.; Shaw, O.; Yao, S.; Berton, L.; Zacharakis, S.; Kim, M.; Heng, H.; Manzano, J. C.; Dobashi, F.; Ng, E.; Ang, S.; Yeo, M.; Colford, C.; Morton, H.; Lazic, O.; Milner, L.; Niazi, S.; Dobashi, F.; Su, E.; Reeder, P.; Milner, L.; Hays, K.; Tseng, T.; Berton, L.; Holmvik, G.; Kerr, S.; Parashar, M.; Goliya, K.; Wells, W.; Fox, J.; Narayanasamy, G.; Carpenter, C.; Leech, J.; Lalor, D.; Rubin, R.; Nayak, D.; Greenhalgh, K.; Pradhan, S.; Glystra, C.; Yennigalla, E.; Bharucha, C.; Rehman, J. *Global Petrochemical Trends*. 2020, No. January, 1−32.

(7) Leippold, M. Trend Derivatives: Pricing, Hedging, and Application to Executive Stock Options. *J. Fut. Mark.* **2018**, *27*, 151−186.

(8) Le Van Mao, R.; Yan, H. T.; Muntasar, A.; Al-Yassir, N. *Blending of Non-Petroleum Compounds with Current Hydrocarbon Feeds to Use in the Thermo-Catalytic Steam-Cracking Process for the Selective Production of Light Olefins*; Elsevier B.V., 2013; 10.1016/B978-0-444-53876-5.00007-6.

(9) Bi, K.; Zhang, S.; Zhang, C.; Li, H.; Huang, X.; Liu, H.; Qiu, T. Knowledge Expression, Numerical Modeling and Optimization Application of Ethylene Thermal Cracking: From the Perspective of Intelligent Manufacturing. *Chin. J. Chem. Eng.* **2021**, *38*, 1−17.

(10) James, C. 12. United States Patent US 6407301 B1, 2002, *1*(12).

(11) Haribal, V. P.; Chen, Y.; Neal, L.; Li, F. Intensification of Ethylene Production from Naphtha via a Redox Oxy-Cracking Scheme: Process Simulations and Analysis. *Engineering* **2018**, *4*, 714−721.

(12) Shelepova, E. V.; Vedyagin, A. A.; Noskov, A. S. Effect of Catalytic Combustion of Hydrogen on Dehydrogenation in a Membrane Reactor. II. Dehydrogenation of Ethane. Verification of the Mathematical Model. *Combust., Explos. Shock Waves* **2013**, *49*, 125−132.

(13) Saito, H.; Sekine, Y. Catalytic Conversion of Ethane to Valuable Products through Non-Oxidative Dehydrogenation and Dehydroaromatization. *RSC Adv.* **2020**, *10*, 21427−21453.

(14) Al-Awadi, A. S.; Al-Zahrani, S. M.; El-Toni, A. M.; Abasaeed, A. E. Dehydrogenation of Ethane to Ethylene by CO2 over Highly Dispersed Cr on Largepore Mesoporous Silica Catalysts. *Catalysts* **2020**, *10*, 97.

(15) Alamdari, A.; Karimzadeh, R.; Abbasizadeh, S. Present State of the Art of and Outlook on Oxidative Dehydrogenation of Ethane: Catalysts and Mechanisms. *Rev. Chem. Eng.* **2021**, *37*, 481−532.

(16) Shelepova, E. V.; Vedyagin, A. A. Intensification of the Dehydrogenation Process of Different Hydrocarbons in a Catalytic Membrane Reactor. *Chem. Eng. Process.* **2020**, *155*, 108072.

(17) Dimitrakopoulos, G.; Schucker, R. C.; Derrickson, K.; Johnson, J. R.; Kopeć, K. K.; Shao, L.; Alahmadi, F.; Ghoniem, A. F. Hydrogen and Ethylene Production through Water-Splitting and Ethane Dehydrogenation Using BaFe 0.9 Zr 0.1 O 3- δ Mixed-Conductors. *ECS Trans.* **2017**, *80*, 181−190.

(18) Schucker, R. C.; Dimitrakopoulos, G.; Derrickson, K.; Kopeć, K. K.; Alahmadi, F.; Johnson, J. R.; Shao, L.; Ghoniem, A. F. Oxidative Dehydrogenation of Ethane to Ethylene in an Oxygen-Ion-Transport-Membrane Reactor: A Proposed Design for Process Intensification. *Ind. Eng. Chem. Res.* **2019**, *58*, 7989−7997.

(19) Gärtner, C. A.; van Veen, A. C.; Lercher, J. A. Oxidative Dehydrogenation of Ethane: Common Principles and Mechanistic Aspects. *ChemCatChem* **2013**, *5*, 3196−3217.

(20) Wang, L. C.; Zhang, Y.; Xu, J.; Diao, W.; Karakalos, S.; Liu, B.; Song, X.; Wu, W.; He, T.; Ding, D. Non-Oxidative Dehydrogenation of Ethane to Ethylene over ZSM-5 Zeolite Supported Iron Catalysts. *Appl. Catal., B* **2019**, *256*, 117816.

(21) Yang, Z.; Li, H.; Zhou, H.; Wang, L.; Wang, L.; Zhu, Q.; Xiao, J.; Meng, X.; Chen, J.; Xiao, F. S. Coking-Resistant Iron Catalyst in Ethane Dehydrogenation Achieved through Siliceous Zeolite Modulation. *J. Am. Chem. Soc.* **2020**, *142*, 16429−16436.

(22) Abashar, M. E. E.; Al-Rabiah, A. A. Production of Ethylene and Cyclohexane in a Catalytic Membrane Reactor. *Chem. Eng. Process.* **2005**, *44*, 1188−1196.

(23) Pang, J.; Zheng, M.; Zhang, T. *Synthesis of Ethanol and Its Catalytic Conversion*, 1st ed.; Elsevier Inc., 2019; Vol. *64*..

(24) Ahn, S. J.; Yun, G. N.; Takagaki, A.; Kikuchi, R.; Oyama, S. T. Effects of Pressure, Contact Time, Permeance, and Selectivity in Membrane Reactors: The Case of the Dehydrogenation of Ethane. *Sep. Purif. Technol.* **2018**, *194*, 197−206.

(25) Hasany, M.; Malakootikhah, M.; Rahmanian, V.; Yaghmaei, S. Effect of Hydrogen Combustion Reaction on the Dehydrogenation of Ethane in a Fixed-Bed Catalytic Membrane Reactor. *Chin. J. Chem. Eng.* **2015**, *23*, 1316−1325.

(26) Amghizar, I.; Vandewalle, L. A.; Van Geem, K. M.; Marin, G. B. New Trends in Olefin Production. *Engineering* **2017**, *3*, 171−178.

https://doi.org/10.1021/acsomega.2c03130
ACS Omega 2022, 7, 28445−28458

(27) Gobina, E.; Hou, K.; Hughes, R. Ethane Dehydrogenation in a Catalytic Membrane Reactor Coupled with a Reactive Sweep Gas. *Chem. Eng. Sci.* **1995**, *50*, 2311−2319.
(28) Palo, E.; Salladini, A.; Morico, B.; Palma, V.; Ricca, A.; Iaquaniello, G. Application of Pd-Based Membrane Reactors: An Industrial Perspective. *Membranes* **2018**, *8*, 101.
(29) Felder, R.; Rousseau, R. *Elementary Principles of Chemical Processes*; Wiley, 2014.
(30) Saeys, M.; Reyniers, M. F.; Neurock, M.; Marin, G. B. Ab Initio Reaction Path Analysis of Catalytic Reactions: Benzene Hydrogenation and Cyclohexane Dehydrogenation. *AIChE Annu. Meet., Conf. Proc.* **2005**, *281*, 11404−11406.
(31) Rahimpour, M. R.; Samimi, F.; Babapoor, A.; Tohidian, T.; Mohebi, S. Palladium Membranes Applications in Reaction Systems for Hydrogen Separation and Purification: A Review. *Chem. Eng. Process.* **2017**, *121*, 24−49.
(32) Jakob, M.; Hawkins, G. A. *Elements of Heat Transfer*; Chapman Hall, 1957; p 317.
(33) Nordio, M.; Soresi, S.; Manzolini, G.; Melendez, J.; Van Sint Annaland, M.; Pacheco Tanaka, D. A.; Gallucci, F. Effect of Sweep Gas on Hydrogen Permeation of Supported Pd Membranes: Experimental and Modeling. *Int. J. Hydrogen Energy* **2019**, *44*, 4228−4239.
(34) Vaswani, S. *Ethylene via Ethane Steam Cracking (29H)*. Process Economics Program, 2014, No. December.
(35) Jenkins, S. 2021 CEPCI updates: April (prelim.) and March (final). https://www.chemengonline.com/2021-cepci-updates-april-prelim-and-march-final/ (accessed May 30, 2022).
(36) MARAFIQ—Customer Relation. Tariff of Water and Electricity. https://www.marafiq.com.sa/en/69-/1/50 (accessed October 21,2021).
(37) Argaam. Petrochemical Index. https://www.argaam.com/ar/sector/petrochemicals/sectorid/33 (accessed October 20, 2021).
(38) Kuenen, H. J.; Mengers, H. J.; Nijmeijer, D. C.; van der Ham, A. G. J.; Kiss, A. A. Techno-Economic Evaluation of the Direct Conversion of CO2 to Dimethyl Carbonate Using Catalytic Membrane Reactors. *Comput. Chem. Eng.* **20162016**, *86*, 136−147.

https://doi.org/10.1021/acsomega.2c03130
ACS Omega 2022, 7, 28445−28458